Electronic Supplementary Information

Growth morphology and symmetry selection of interfacial instabilities in anisotropic environments

Qing Zhang,[a] Amin Amooie,[b] Martin Z. Bazant,[b,c] and Irmgard Bischofberger[*a]

1 Parameters used in the experiments

Table S1 reports the composition of the water-glycerol mixtures used in the experiments, and the values of the viscosity ratios η_{in}/η_{out}, the viscosities of the inner fluids η_{in} and the viscosities of the outer fluids η_{out}.

Table S2 reports the flow rate q, the channel depth h, the plate spacing b and the viscosity ratio η_{in}/η_{out} for each experiment.

2 Negligible effects of diffusion in the numerical simulations

The numerical simulations are governed by the second-order advection-diffusion transport equation, and in accordance with the experiments the simulations are performed in the high Péclet number regime where advection dominates over diffusive effects. We confirm this by varying the diffusion coefficient by several orders of magnitude and showing that the pattern morphology is independent of the diffusion coefficient (or equivalently of a dimensionless Péclet number) over eight orders of magnitude, as shown in Fig. S1. At low enough Péclet number, diffusive effects dominate the pattern growth and stabilize the instability. All the simulations reported in the manuscript are performed far from this low Péclet number regime.

To provide a dimensionless point of reference, we define the Péclet number as Pe $= UL/D$, where U is the characteristic velocity, L is a characteristic length scale and D is the diffusion coefficient[1]. For a radial flow, Pe $= Q/D$ has been used[2,3] with Q [m²/s] the gap-averaged flow rate, i.e. the volumetric flow rate per unit depth. As discussed in[4], this implies that the characteristic velocity for radial source flows is $U = Q/L$, where L is the distance from the center of the cell. For a con-

stant injection rate and a *stable* displacement, $U \propto 1/L$ and UL is equal to Q at any point. However, this equality and hence the applicability of the expression Pe $= Q/D$ holds only for a stable radial flow propagation. When instabilities are present, the velocity does not vary as $1/L$ and UL at a finger tip can be larger than Q. Pe $= Q/D$ therefore provides a lower bound for radial flows subject to viscous fingering instabilities. Keeping this in mind, we now use this definition of Pe.

The injection velocity is set to 0.14 m/s and imposed on an inner circle (inlet hole) of radius 1.4 mm. This gives a depth-averaged $Q \sim 0.0002$ m²/s, comparable to the depth-averaged Q used in the experiments ranging from 0.00012 to 0.0033 m²/s. We have confirmed that UL at any point beyond the injection source and sufficiently behind the unstable interface maintains this value, but it increases at a finger tip. Given a certain diffusion coefficient and Q, we can estimate a lower bound for the Péclet number. For instance, a Péclet number $\sim O(1)$ required to suppress the instability[2] in an *isotropic* system would imply a diffusion coefficient $\sim 10^{-4}$ m²/s, in good agreement with our value of $\sim 10^{-5}$ m²/s for an *anisotropic* system reported in Fig. S1. Exploring the stabilizing effect of diffusion on the transition between dendritic and dense-branching growth in anisotropic media is an exciting line of future research.

3 Convergence of the numerical simulations

We have paid careful attention to the robustness and validity of the numerical modeling and have confirmed the numerical convergence, as demonstrated in Fig. S2. An optimal numerical mesh is chosen such that the fine features of the domain are well discretized, the simulations are computationally feasible, and a good degree of convergence is achieved in the flow dynamics and the pattern morphology. The optimal mesh that meets these criteria consists of 222,162 triangular elements that discretize an annular mesh area encompassing arrays of triangular objects. The average mesh element quality is above 0.9 with respect to various mesh quality measures including skewness, maximum angle, and growth rate of elements. The mesh element quality is a dimensionless quantity

[a] Department of Mechanical Engineering, Massachusetts Institute of Technology, Cambridge, MA 02139, USA. E-mail: irmgard@mit.edu
[b] Department of Chemical Engineering, Massachusetts Institute of Technology, Cambridge, MA 02139, USA.
[c] Department of Mathematics, Massachusetts Institute of Technology, Cambridge, MA 02139, USA.

between 0 and 1, where 1 represents a perfectly regular element and 0 represents a degenerated element. A larger than 0.9 mesh quality represents a geometrically well-behaved and high-quality mesh that facilitates numerical convergence.

4 Movies showing the growth of dendritic patterns

The movies show the growth of dendritic patterns resulting from the displacement of a more-viscous fluid by a less-viscous one in the anisotropic environment of six-fold symmetric lattice channels. The width of the lattice channels is $w = 800$ μm, the distance between the edges of two channels is $d = 850$ μm. The flow rate is $q = 1$ ml/min, the channel height is $h = 250$ μm, and the plate spacing between the engraved acrylic plate and the top glass plate is $b = 508$ μm.

Movie 1: The viscosity ratio between the inner and the outer fluid is $\eta_{in}/\eta_{out} = 0.0013$. The pattern exhibits six-fold symmetry.

Movie 2: The viscosity ratio between the inner and the outer fluid is $\eta_{in}/\eta_{out} = 0.05$. Both main and sub dendrites grow at comparable rates.

5 Symmetry of dendritic patterns depends on the degree of anisotropy h/b

For a fixed viscosity ratio η_{in}/η_{out}, a decrease in the degree of anisotropy h/b leads to a systematic transition from six- towards twelve-fold symmetric dendrites, as shown in Fig. S3 for $\eta_{in}/\eta_{out} = 0.0125$ and a flow rate of 1 ml/min.

6 Simplified model to account for the effect of the degree of anisotropy and the viscosity ratio on the pattern growth

Our experiments and simulations reveal that the degree of anisotropy h/b and the viscosity ratio η_{in}/η_{out} govern the growth of the sub and main dendrites in an anisotropic environment. We simplify our topology by considering flow in two directions with respect to the direction of parallel engraved channels, to capture the role of h/b and η_{in}/η_{out} in governing the pattern growth: (a) the pressure gradient ∇p is parallel to the channels, corresponding to the growth of the main dendrites and (b) the pressure gradient ∇p is perpendicular to the channels, representing the growth of the sub dendrites, as shown in Figs. S4a and S4b. We note that such a texture, as well as that of our more complex six-fold symmetric lattice, is isotropic for a single-phase flow. For a two-phase flow, however, the presence of the interface leading to a gradient of viscosity in the flow direction can locally break the symmetry

and lead to an anisotropic two-phase permeability of the interface region. To account for this, we use concepts derived for the hydrodynamics of slippage on textured surfaces for two-phase flows over hydrophobic surfaces[5,6]. In analogy to these concepts, and to account for the local asymmetry, we consider that the more-viscous outer fluid can get partially trapped in the channels as the less-viscous fluid flows above the texture following the path of least resistance, as schematically shown in Fig. S4c. This conceptualization allows us to introduce a local effective slip length to model the interface region[5,7–10].

We denote the height of the layer of trapped outer fluid as $\delta = \alpha h$, where α denotes a direction-dependent coefficient. The local effective slip length felt by the inner fluid over a valley of height h, measured from the no-slip boundary at the surface of the channel-free region (dashed line in Fig. S4c), scales as

$$b_{\text{slip}} = h - \delta \left(1 - \frac{\eta_{\text{in}}}{\eta_{\text{out}}} \right) = h - \alpha h \left(1 - \frac{\eta_{\text{in}}}{\eta_{\text{out}}} \right) \quad \text{(S1)}$$

The enhancement of permeability due to b_{slip} scales as

$$\frac{b_{\text{slip}}}{b} = \frac{h}{b} - \frac{h}{b}\alpha \left(1 - \frac{\eta_{\text{in}}}{\eta_{\text{out}}} \right) \quad \text{(S2)}$$

For single-phase flow, where $\eta_{\text{in}}/\eta_{\text{out}} = 1$, $b_{\text{slip}} = h$ and the permeability above the channel is proportional to $h + b$. For two-phase flow, however, b_{slip} decreases with decreasing viscosity ratio leading to a smaller enhancement of the permeability. The decrease of b_{slip} depends on the direction of the channels with respect to the flow, leading to a local symmetry breaking and the rich anisotropic pattern selection.

When $\text{Tr}(\mathbf{b}_{\text{slip}})/b \gg 1$, the effect of the channels dominates and an analysis in terms of an effective slip tensor is not applicable. The case of interest here is when $\text{Tr}(\mathbf{b}_{\text{slip}})/b \ll 1$, where the texture can be analyzed locally in terms of an effective slip tensor. This effective slip tensor is positive definite and 90° symmetric between the fast and slow directions[9,11],

$$\mathbf{b}_{\text{slip}} = \mathbf{S}_\theta \begin{pmatrix} b_{\text{slip},\parallel} & 0 \\ 0 & b_{\text{slip},\perp} \end{pmatrix} \mathbf{S}_{-\theta} \quad \text{(S3)}$$

where $\mathbf{S}_\theta = \begin{pmatrix} \cos\theta & \sin\theta \\ -\sin\theta & \cos\theta \end{pmatrix}$ and θ is the angle between the pressure gradient and the texture. $b_{\text{slip},\parallel}$, $b_{\text{slip},\perp}$ are two eigenvalues of $\mathbf{b}_{\text{slip}}$. The subscripts $\parallel, \perp$ denote the fast direction and the slow direction, respectively. Note that here, the fast direction of the effective slip tensor corresponds to the direction of the main dendrites, the slow direction corresponds to the direction of the sub dendrites. The two corresponding eigenvectors have a 90° symmetry[11], corresponding to the formation of, respectively, the main dendrites at 0°, 60°, 120° and the sub dendrites at 30°, 90°, 150°.

From Eq. (S1), we have

$$b_{\text{slip},\parallel} = h \left(1 - \alpha_\parallel + \alpha_\parallel \frac{\eta_{\text{in}}}{\eta_{\text{out}}} \right) \tag{S4}$$

and

$$b_{\text{slip},\perp} = h \left(1 - \alpha_\perp + \alpha_\perp \frac{\eta_{\text{in}}}{\eta_{\text{out}}} \right) \tag{S5}$$

where $\alpha_{\parallel,\perp}$ denotes the coefficient for the fast and slow direction, respectively, related to the effective slip tensor. As $b_{slip,\parallel} > b_{slip,\perp}$, we have $\alpha_\perp > \alpha_\parallel$.

The dimensionless effective permeability tensor, scaled to its value without slip, is expressed as

$$\mathbf{K} = \mathbf{I} + 3\mathbf{A_p} \tag{S6}$$

where $\mathbf{A_p}$ is a dimensionless matrix describing a slip-driven plug flow in the $\mathbf{A_p}\nabla p$ direction [11]. We have

$$\mathbf{A_p} = \mathbf{S}_\theta \begin{pmatrix} A_s\left(b_\parallel\right) & 0 \\ 0 & A_s\left(b_\perp\right) \end{pmatrix} \mathbf{S}_{-\theta} \tag{S7}$$

where $A_s\left(b_{\perp,\parallel}\right) = \frac{b_{\perp,\parallel}}{b + b_{\perp,\parallel}}$. For $\theta = 0°$, this gives

$$\mathbf{K} = \begin{pmatrix} K_{xx} & K_{xy} \\ K_{yx} & K_{yy} \end{pmatrix} = \begin{pmatrix} 1 + \frac{3}{\frac{b}{b_{\text{slip},\parallel}}+1} & 0 \\ 0 & 1 + \frac{3}{\frac{b}{b_{\text{slip},\perp}}+1} \end{pmatrix} \tag{S8}$$

Substituting Eq. (S4) and Eq. (S5) into Eq. (S8) yields

$$\mathbf{K} = \begin{pmatrix} 1 + \frac{3}{\frac{b}{h\left(1-\alpha_\parallel + \alpha_\parallel \frac{\eta_{\text{in}}}{\eta_{\text{out}}}\right)}+1} & 0 \\ 0 & 1 + \frac{3}{\frac{b}{h\left(1-\alpha_\perp + \alpha_\perp \frac{\eta_{\text{in}}}{\eta_{\text{out}}}\right)}+1} \end{pmatrix} \tag{S9}$$

For our case where $b_{\text{slip}}/b \ll 1$, the effective permeability tensor can be expressed as

$$\kappa \approx \frac{b^2}{12\eta_{\text{in}}} \begin{pmatrix} 1 + \frac{3h\left(1-\alpha_\parallel + \alpha_\parallel \frac{\eta_{\text{in}}}{\eta_{\text{out}}}\right)}{b} & 0 \\ 0 & 1 + \frac{3h\left(1-\alpha_\perp + \alpha_\perp \frac{\eta_{\text{in}}}{\eta_{\text{out}}}\right)}{b} \end{pmatrix} \tag{S10}$$

For the simplified topology in Fig. S4, the main dendrites form along the fast direction of the effective permeability and the sub dendrites form along the slow direction of the effective permeability:

$$\kappa_{\text{m}} = \frac{b^2}{12\eta_{\text{in}}} K_{xx} \approx \frac{b^2}{12\eta_{\text{in}}} \left(1 + \frac{3h}{b}\left(1 - \alpha_\parallel + \alpha_\parallel \frac{\eta_{\text{in}}}{\eta_{\text{out}}}\right) \right) \tag{S11}$$

$$\kappa_{\text{s}} = \frac{b^2}{12\eta_{\text{in}}} K_{yy} \approx \frac{b^2}{12\eta_{\text{in}}} \left(1 + \frac{3h}{b}\left(1 - \alpha_\perp + \alpha_\perp \frac{\eta_{\text{in}}}{\eta_{\text{out}}}\right) \right) \tag{S12}$$

This shows that as $\eta_{\text{in}}/\eta_{\text{out}}$ increases, the effective permeabilities in the main and sub channels, κ_{m} and κ_{s}, increase. Accordingly, the interface velocities in the main and sub channels, $\mathbf{u}_{\text{m}} = -\kappa_{\text{m}}\nabla p$ and $\mathbf{u}_{\text{s}} = -\kappa_{\text{s}}\nabla p$, increase. Let us now discuss the role of the viscosity ratio $\eta_{\text{in}}/\eta_{\text{out}}$ for the increase in permeability for both the main dendrites and the sub dendrites.

The ratio of the derivatives of the permeability for sub dendrites and main dendrites is

$$\frac{\partial \kappa_{\text{s}}/\partial\left(\eta_{\text{in}}/\eta_{\text{out}}\right)}{\partial \kappa_{\text{m}}/\partial\left(\eta_{\text{in}}/\eta_{\text{out}}\right)} \sim \frac{\alpha_\perp}{\alpha_\parallel} > 1 \tag{S13}$$

Therefore, for increasing viscosity ratio, the increase in permeability along the sub dendrites (slow direction) is larger than the increase in permeability along the main dendrites (fast direction).

The ratio of the interface velocities between the sub dendrites and the main dendrites scales as

$$\frac{u_{\text{s}}}{u_{\text{m}}} \simeq \frac{\kappa_{\text{s}}}{\kappa_{\text{m}}} \simeq 1 - \frac{3\left(1 - \frac{\eta_{\text{in}}}{\eta_{\text{out}}}\right)\left(\alpha_\perp - \alpha_\parallel\right)}{\frac{b}{h} + 3\left(1 - \alpha_\parallel\left(1 - \frac{\eta_{\text{in}}}{\eta_{\text{out}}}\right)\right)} \tag{S14}$$

where $\alpha_\perp - \alpha_\parallel \geq 0$.

This analysis shows that for the case of $b_{\text{slip}}/b \ll 1$, $u_{\text{s}}/u_{\text{m}}$ increases with an increase in the viscosity ratio $\eta_{\text{in}}/\eta_{\text{out}}$ or a decrease in the degree of anisotropy h/b. When the viscosity ratio $\eta_{\text{in}}/\eta_{\text{out}}$ approaches 1, $u_{\text{s}}/u_{\text{m}}$ will be close to 1. When h/b approaches zero, $u_{\text{s}}/u_{\text{m}}$ approaches 1. Clearly, this description is oversimplified but it does capture the essential features of how the viscosity ratio $\eta_{\text{in}}/\eta_{\text{out}}$ and the degree of anisotropy h/b affect the interface velocities of the main and sub dendrites, and therefore the growth of R_{m} and R_{s}.

7 Growth of sub dendrites

At early stage, two fingers grow between pairs of neighboring main dendrites on each side of the 30° direction to the straight channels, as shown in Fig. S5a. This is observed at any viscosity ratio. At low viscosity ratio and large h/b, these fingers soon merge with the main dendrites, which results in a six-fold symmetric pattern. With increasing $\eta_{\text{in}}/\eta_{\text{out}}$ and decreasing h/b, each of the two fingers will further split into two as they reach the next lattice junction. One branch advances parallel to the main dendrite and eventually merges with it. The other branch diverts towards the 30° direction and will merge with its counterpart on the other side of the 30° direction into a sub dendrite, as shown in Fig. S5b. Depending on which finger grew slightly faster, the sub dendrite will grow in a zig-zag path along the 30° direction either right below or above this direction, as illustrated by the arrows in Fig. S5c and Fig. S5a. The absence of interfacial tension implies that

the flow is unaffected by pinning effects on corners that become important in immiscible fluids[12,13]. As a result, when the tip of a sub dendrite reaches an entrance of a junction, as shown in the schematics of the zoomed-in region in Fig. S6b, its path is governed by the combination of the global pressure distribution from the main dendrites and the local pressure distribution from the tip of the sub dendrites.

When the tip of a sub dendrite reaches a junction that is not on the 30° line, indicated by a green dot in Fig. S6a, the pressure profile in the outer fluid imposed by the main dendrites pushes the tip predominantly towards the 30° line through channel 1. When the tip of a sub dendrite reaches a junction on the 30° line through channel 4, indicated by a cyan dot in Fig. S6a, it grows towards channel 2 as the local pressure field at the tip is biased towards its initial side of the 30° line, where it first started to grow. Note that in Fig. S6a, we differentiate between these two sides by the pink and yellow arrows; the sub dendrite follows either the yellow or the pink zig-zag path depending on the side it first appeared.

We note that a small amount of fluid also goes towards the direction that is not selected by the sub dendrite tip (channel 1 from the cyan dot for an incoming liquid through the horizontal channel 4, for example). This flow leads to the side-branch decoration along the sub dendrites.

References

1 G. M. Homsy, *Annu. Rev. Fluid Mech*, 1987, **19**, 271–311.

2 C. T. Tan and G. M. Homsy, *Phys. Fluids*, 1987, **30**, 1239–1245.

3 V. Sharma, S. Nand, S. Pramanik, C.-Y. Chen and M. Mishra, *J. Fluid Mech.*, 2020, **884**, A16.

4 A. Riaz and E. Meiburg, *Phys. Fluids*, 2003, **15**, 938–946.

5 O. I. Vinogradova, *Int. J. Miner. Process.*, 1999, **56**, 31–60.

6 F. Feuillebois, M. Z. Bazant and O. I. Vinogradova, *Phys. Rev. Lett.*, 2009, **102**, 026001.

7 A. D. Stroock, S. K. Dertinger, G. M. Whitesides and A. Ajdari, *Anal. Chem.*, 2002, **74**, 5306–5312.

8 H. A. Stone, A. D. Stroock and A. Ajdari, *Annu. Rev. Fluid Mech.*, 2004, **36**, 381–411.

9 S. Schmieschek, A. V. Belyaev, J. Harting and O. I. Vinogradova, *Phys. Rev. E*, 2012, **85**, 016324.

10 K. Kamrin, M. Z. Bazant and H. A. Stone, *J. Fluid Mech.*, 2010, **658**, 409–437.

11 M. Z. Bazant and O. I. Vinogradova, *J. Fluid Mech.*, 2008, **613**, 125–134.

12 A. G. Banpurkar, A. S. Ogale, A. V. Limaye and S. B. Ogale, *Phys. Rev. E*, 1999, **59**, 2188–2191.

13 A. G. Banpurkar, A. V. Limaye and S. B. Ogale, *Phys. Rev. E*, 2000, **61**, 5507–5511.

Table S1 Composition and viscosities of the water-glycerol mixtures

c_{glycerol} (wt%)	$\eta_{\text{in}}/\eta_{\text{out}}$	η_{in} (Pa s)	η_{out} (Pa s)
0	0.0011	0.0013	1.176
12.3	0.0013	0.0015	1.176
39.1	0.0025	0.0029	1.176
52.9	0.005	0.0059	1.176
59.6	0.0075	0.0088	1.176
63.4	0.0125	0.0147	1.176
72.4	0.0234	0.0275	1.176
76.6	0.03	0.0351	1.176
79	0.04	0.0468	1.176
81.3	0.05	0.0592	1.176
84.4	0.068	0.08	1.176
86.8	0.1	0.118	1.176
89.9	0.157	0.185	1.176

Table S2 Parameters used in the experiments

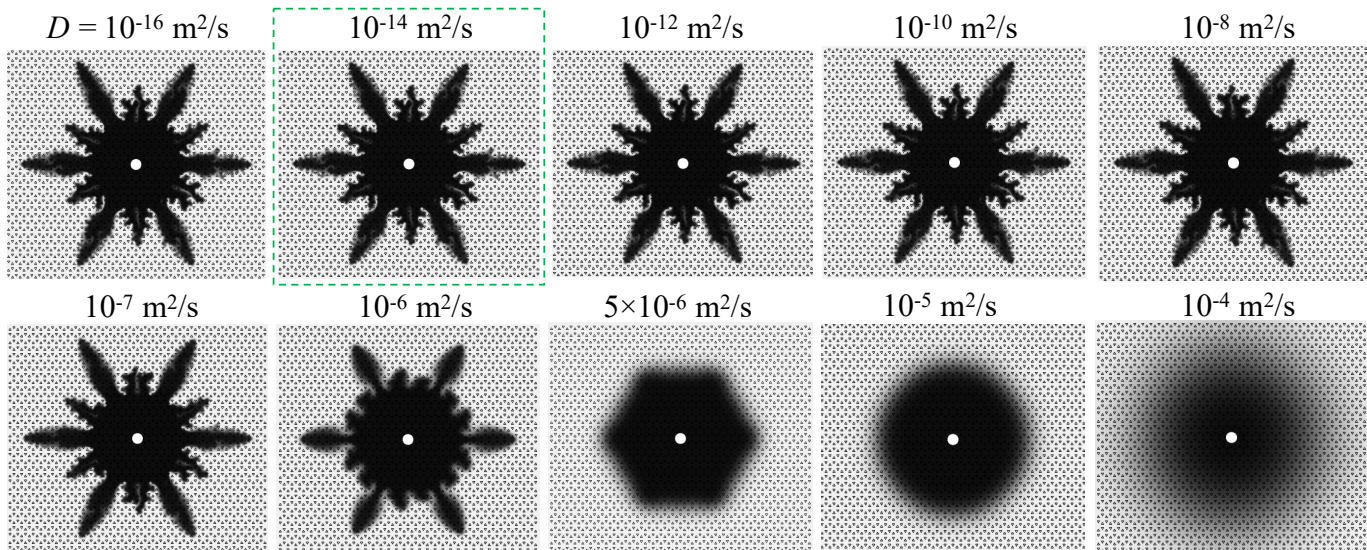| h (μm)	$\eta_{\text{in}}/\eta_{\text{out}}$	$q = 1$ ml/min						$q = 10$ ml/min	
		b (mm)	b (μm)	b (μm)	b (μm)	b (μm)	b (μm)	b (μm)	b (μm)
10	0.0013	254							
28	0.0013	762	508	254	203	127		762	
	0.0025							762	
	0.03	762	508	254	127				
	0.005							508	
	0.068	762						508	
50	0.0011	508	254						
	0.0013	1000	762	508	127	100	55	762	508
	0.0025	1000	508	254					
	0.005	1000	508	254					
	0.0075	508	254						
	0.0125	1000	508	254				762	
	0.0234	1000	762	508	203				
	0.03	254							
	0.05	1000	762	508	254	203			
	0.068	1350	375	254				508	
250	0.0013	1000	762	508	254	127		508	
	0.0025	508	254						
	0.005	762	508	254					
	0.0075	762							
	0.0125	762	508	254				508	
	0.0234	762	508	203				508	
	0.03	508	254						
	0.04	508	762					508	
	0.05	508	508	254				508	
	0.068	508						508	
	0.1	508	762						
	0.157	508							

Fig. S1 Simulated patterns ($\eta_{in}/\eta_{out} = 0.05$ and $h/b = 0.49$) obtained for different diffusion coefficients D. The dashed box denotes the conditions used in the manuscript.
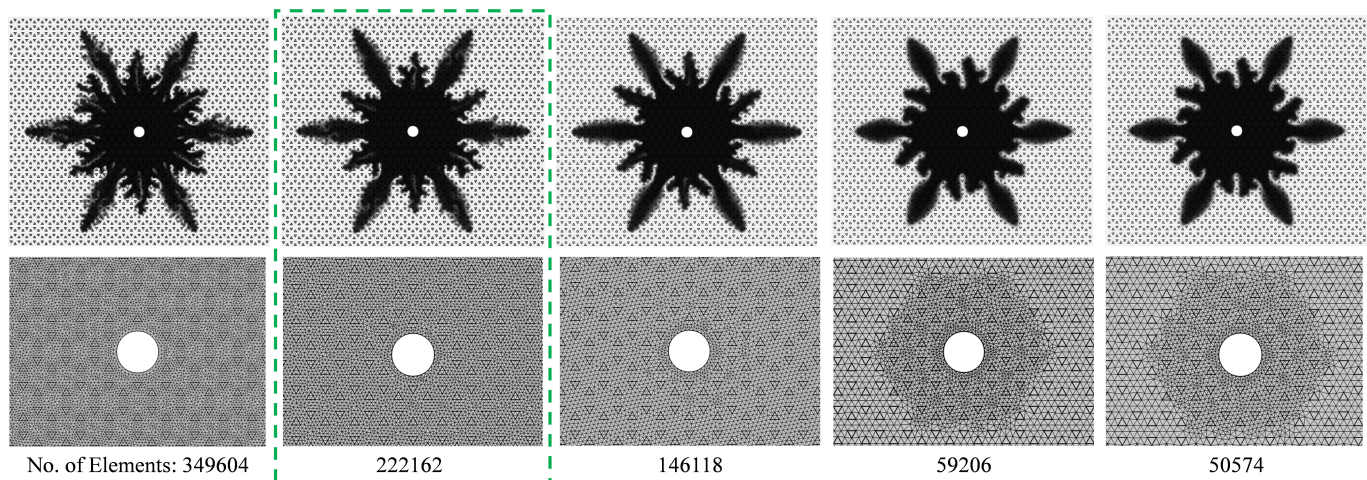

Fig. S2 Simulated patterns ($\eta_{in}/\eta_{out} = 0.05$, $h/b = 0.49$) for different mesh resolutions. The mesh used for the results reported in the manuscript is denoted by the dashed box.
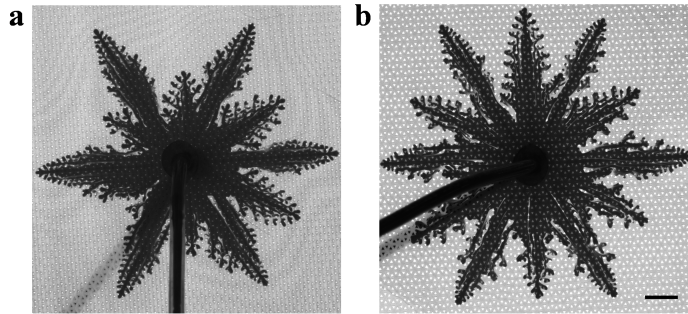
Fig. S3 Dendritic patterns formed at $\eta_{\text{in}}/\eta_{\text{out}} = 0.0125$ for (a) $h/b = 1$ and (b) $h/b = 0.2$. The scale bar is 1 cm.
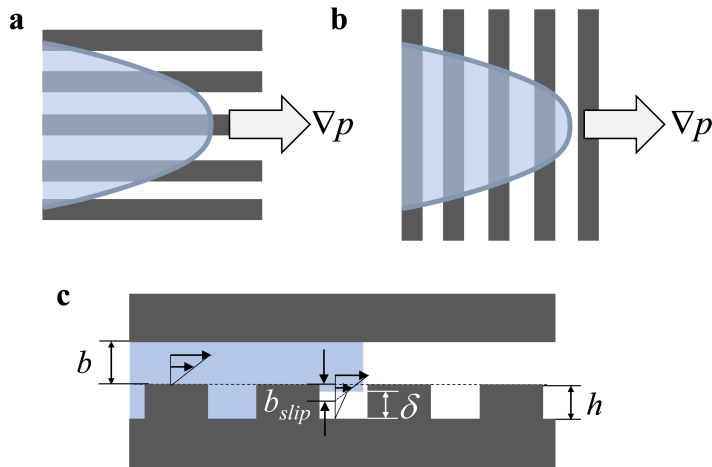

Fig. S4 Schematic of the simplified channel texture. (a) The main dendrites grow along channels parallel to the flow direction. (b) The sub dendrites grow along channels perpendicular to the flow direction. (c) The effective slip length b_{slip} at the interface between the two fluids modifies the local permeability as the inner fluid flows above the channels. The light blue region represents the less-viscous inner fluid, the white region represents the more-viscous outer fluid within the channel.
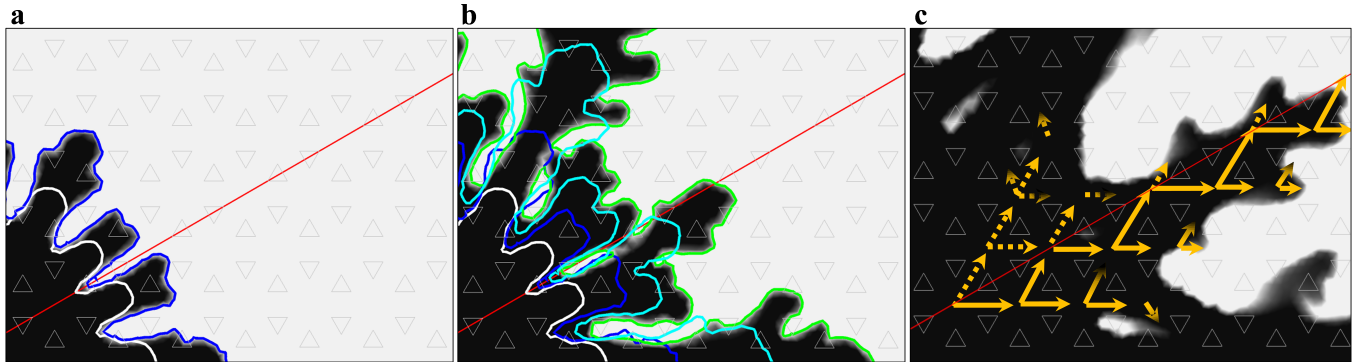
Fig. S5 Formation and growth of sub dendrites. (a) At early stage, two fingers emerge between the neighboring main dendrites (white contour). They further split as they reach the center of a next lattice (blue contour). (b) One of the fingers outgrows the other one and becomes a sub dendrite (in this example, the one below the red 30° line). The colored contours represent the interface position at different times. (c) The sub dendrite further grows along the zig-zag path illustrated by the solid yellow arrows. A smaller amount of flow also goes towards the dashed yellow arrows, leading to the formation of side branches.
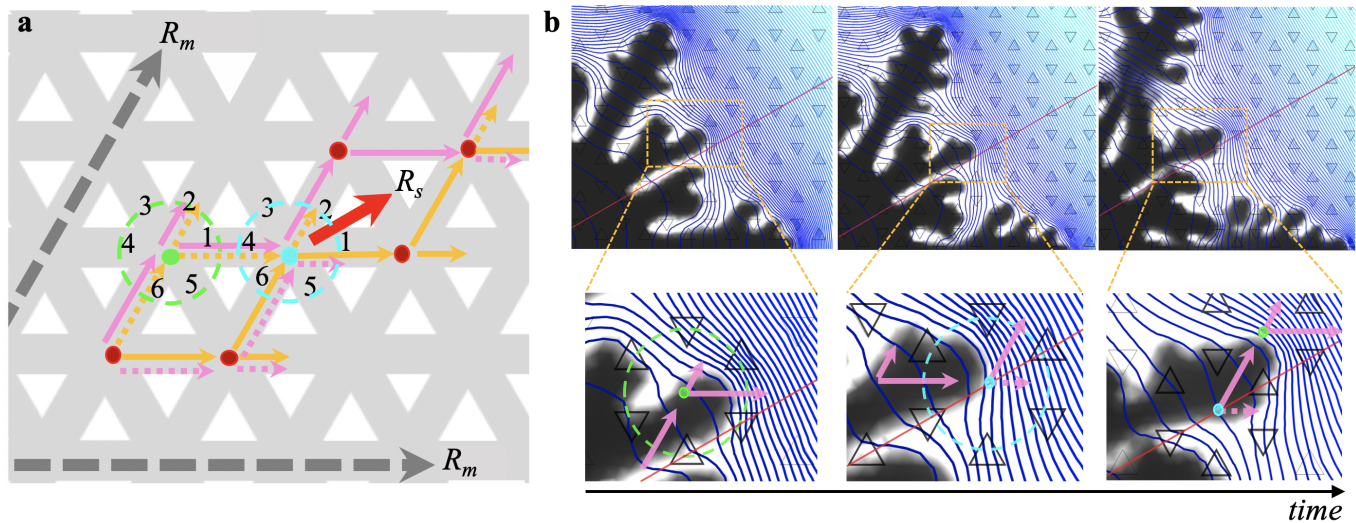

Fig. S6 Path selection towards 30° direction governed by pressure profile. (a) As the tip of a sub dendrite reaches a junction that is *not* on the 30° line, indicated by a green dot, the pressure profile in the outer fluid imposed by the two neighboring main dendrites pushes the tip towards the 30° line through channel 1, as shown in the left inset of (b). As the tip reaches a junction *on* the 30° line, indicated by a cyan dot, through channel 4, it grows towards channel 2 because the local pressure gradient is highest in that direction, as shown in the middle inset of (b). The sub dendrite continues to grow on the same side of the 30° line where it first developed. The pink arrows denote the path of a sub dendrite formed above the 30° line, the yellow arrows denote the path of a sub dendrite formed below the 30° line. The solid arrows indicate the main direction of the flow, but a small amount of flow goes towards the dashed arrows and leads to the side-branch decoration of the dendrites.